

# SPONTANEOUS CURRENT-LAYER FRAGMENTATION AND CASCADING RECONNECTION IN SOLAR FLARES: I. MODEL AND ANALYSIS

MIROSLAV BÁRTA<sup>1,2</sup>, JÖRG BÜCHNER<sup>1</sup>, MARIAN KARLICKÝ<sup>2</sup>, AND JAN SKÁLA<sup>2,3</sup>

<sup>1</sup>Max Planck Institute for Solar System Research, D-37191 Katlenburg-Lindau, Germany

<sup>2</sup>Astronomical Institute of the Academy of Sciences of the Czech Republic, CZ-25165 Ondřejov, Czech Republic

<sup>3</sup>University of J.E. Purkinje, CZ-40096 Ústí nad Labem, Czech Republic

*Draft version October 8, 2018*

## ABSTRACT

Magnetic reconnection is commonly considered as a mechanism of solar (eruptive) flares. A deeper study of this scenario reveals, however, a number of open issues. Among them is the fundamental question, how the magnetic energy is transferred from large, accumulation scales to plasma scales where its actual dissipation takes place. In order to investigate this transfer over a broad range of scales we address this question by means of a high-resolution MHD simulation. The simulation results indicate that the magnetic-energy transfer to small scales is realized via a cascade of consecutive smaller and smaller flux-ropes (plasmoids), in analogy with the vortex-tube cascade in (incompressible) fluid dynamics. Both tearing and (driven) “fragmenting coalescence” processes are equally important for the consecutive fragmentation of the magnetic field (and associated current density) to smaller elements. At the later stages a dynamic balance between tearing and coalescence processes reveals a steady (power-law) scaling typical for cascading processes. It is shown that cascading reconnection also addresses other open issues in solar flare research such as the duality between the regular large-scale picture of (eruptive) flares and the observed signatures of fragmented (chaotic) energy release, as well as the huge number of accelerated particles. Indeed, spontaneous current-layer fragmentation and formation of multiple channelised dissipative/acceleration regions embedded in the current layer appears to be intrinsic to the cascading process. The multiple small-scale current sheets may also facilitate the acceleration of a large number of particles. The structure, distribution and dynamics of the embedded potential acceleration regions in a current layer fragmented by cascading reconnection are studied and discussed.

*Subject headings:* Sun: flares — Acceleration of particles — Magnetic reconnection — Magnetohydrodynamics (MHD) — Turbulence

## 1. INTRODUCTION

It is generally conjectured that solar flares represent a dissipative part of the release of the magnetic energy accumulated in active regions at the Sun. The ‘standard’ CSHKP model (see, e.g. Shibata & Tanuma 2001; Mandrini 2010; Magara et al. 1996, and references therein) agrees well with the observed large-scale dynamics of eruptive events. In this model the flares are initiated by eruption of a flux-rope (in many cases observed as a filament) via, for example, a kink or torus instability (e.g. Kliem & Török 2006; Török & Kliem 2005; Williams et al. 2005; Kliem et al. 2010) evolving later into a Coronal Mass Ejection (CME). The latter is trailed by a large-scale current layer behind the ejecta (Lin & Forbes 2000). In this trailing current layer reconnection is supposed to give rise to various observed phenomena like hot SXR/EUV flare loops rooted in H $\alpha$  chromospheric ribbons, HXR sources in loop-top and foot-points, and radio emissions of various types. Some authors (e.g. Ko et al. 2003; Lin et al. 2007) argue that the bright thin ray-like structure observed sometimes behind CMEs may represent a manifestation of the density increase connected with this current sheet (CS).

However, closer analysis of the classical CSHKP model revealed some of its open issues. Namely, the time-scales of reconnection in such a thick flare CS appeared to be

much longer than typical flare duration. In other words, reconnection rate in such configurations has been found to be insufficient for the rapid energy release observed in flares. Later it was found that the dissipation necessary for reconnection in the practically collisionless solar corona is an essentially plasma-kinetic process (see, e.g., Büchner 2006) which takes place at very small spatial scales. Hence, the question arises, how sufficiently thin CSs can build up within the global-scale, thick CME-trailing current layer: Open is the actual physical mechanism that provides the energy transfer from the global scales, at which the energy is accumulated to the much smaller scales, at which the plasma-kinetic dissipation takes place.

Addressing these questions Shibata & Tanuma (2001) suggested a concept of cascading (or *fractal*, as they call it) reconnection. According to their scenario a cascade of non-linear tearing instabilities occurs in the continuously stretched current layer formed behind a CME. Multiple magnetic islands (helical flux-ropes in 3D), also called plasmoids, are formed, interleaved by thin CSs. Due to increasing separation of the plasmoids in the continuously vertically extending trailing part of the CME the interleaving CSs are subjected to further filamentation until the threshold for secondary tearing instability is reached. This process continues further, third and higher levels of tearing instabilities take place, until the width of the CSs reaches the kinetic scale.

This scenario has recently been supported by the analytical theory of *plasmoid instability* by Loureiro et al. (2007). They show that the high-Lundquist-number systems with high enough current-sheet length-to-width ratio are not subjected to the slow Sweet-Parker reconnection but they are inherently unstable to formation of plasmoids on very short time-scales. Samtaney et al. (2009), Bhattacharjee et al. (2009), and Huang & Bhattacharjee (2010) confirmed predictions of this analytical theory by numerical simulations with high Lundquist numbers. Ni et al. (2010) generalizes the model by presence of shear flows around current sheet (CS). Uzdensky et al. (2010) relate the theory of plasmoid instability further to the concept of fractal reconnection suggested by Shibata & Tanuma (2001). Shepherd & Cassak (2010) and Huang et al. (2010) study the plasmoid instability numerically at smaller scales and investigate its relation to the Hall reconnection. They found various regimes of parameters where different type of reconnection prevails.

Eventually, however, kinetic scales are reached where dissipation and particle acceleration take place most likely via kinetic coalescence of micro-plasmoids and, possibly, their shrinkage (Drake et al. 2005; Karlický & Bárta 2007; Karlický et al. 2010).

In addition to the issue of energy transport there are also other questions that remain open in the CSHKP model. It is its apparent insufficiency to accelerate such a number of particles in its single diffusion region around the X-line that would correspond to the fluxes inferred from HXR observations in the thick-target model (Fletcher 2005; Krucker et al. 2008, and references therein). And, furthermore, the HXR and radio (e.g. decimetric spikes, see Karlický et al. 1996, 2000; Bárta & Karlický 2001) observations indicate that the particle acceleration takes place via multiple concurrent small-scale events distributed chaotically in the flare volume rather than by a single compact acceleration process hosted by a single diffusion region. Such observations are usually referred to as signatures of fragmented/chaotic energy release in flares.

Because of these difficulties an alternative concept based on the so-called “self-organized criticality” (SOC) has been proposed (Aschwanden 2002; Vlahos 2007). This class of models is based on the idea of multiple small-scale CSs embedded in chaotic (braided) magnetic fields that are formed as a consequence of random motions at the system boundary (photosphere). Multiple CSs can host multiple reconnection sites what provides natural explanation of observed signatures of fragmented energy release. At the same moment they provide larger total volume of diffusion regions, perhaps sufficient to account for the observed particle fluxes also quantitatively. Organised large-scale picture (i.e. coherent structures like the flare-loop arcades) should be in the case of SOC-based models achieved by the so-called avalanche principle: A small-scale energy release event can trigger similar events in its vicinity provided the system is in marginally stable state (due to the continuous pumping of energy and entropy through the boundary). Nevertheless, it is difficult to achieve such coherent large-scale structures as they are usually observed in solar flares in the frame of SOC-based models.

Thus, solar flares appear to be enigmatic phenomena

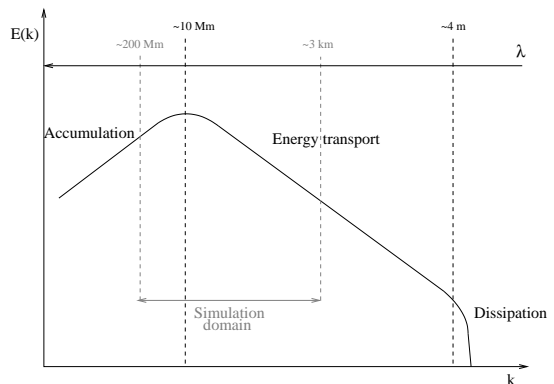


FIG. 1.— Large-scale magnetic reconnection from the point of view of theory of dynamical systems. Schematic view of the cascade of energy transfer from large to small scales and the window of scales resolved in our simulations. Lower abscissa shows the wave number  $k$ , corresponding characteristic scales  $\lambda = 2\pi/k$  are at the upper abscissa. The numeric values at the scale axis correspond to scaling based on typical coronal parameters (for details on scaling see Section 2).

exhibiting duality between the regular, well-organized dynamics of flares observed at large scales and signatures of fragmented/chaotic energy release seen in observations related to flare-accelerated particles. While the coherent global eruption (flare) picture seems to be in agreement with the CSHKP scenario, the observed fragmented-energy-release signatures favor the SOC-based class of models.

In the present paper, we suggest that cascading reconnection can address these three pressing questions (i.e. energy transport across the scales, accelerated-particles fluxes, and the organized/chaotic picture duality) as closely related to each other. In our view the energy is transferred from large to small scales by the cascade of fragmentation of originally large-scale magnetic structures to smaller elements. We identify two elementary processes of this fragmentation (see Section 3). In the course of this process also the initial current layer fragments into multiple small-scale, short-living current sheets. These current sheets are hierarchically embedded inside the thick current layer in qualitatively self-similar manner. In this sense the cascading fragmentation reminds SOC models, but now the chaotic distribution of small-scale currents results from *internal* instabilities of the global current layer. The fragmented current layer represents the modification of the standard CSHKP model and thus it keeps coherent large-scale picture of solar flares. At the same time it addresses the observed signatures of fragmented energy release and the question of efficient particle acceleration. We believe that the cascading reconnection in solar coronal current layers can thus address the three main problems mentioned above *en bloc*, and it reconciles the two concepts of the standard CSHKP and SOC-based models seen hitherto as antagonistic.

The paper is organized as follows: First, we describe the model used in our investigations. Then we present results of our high-resolution MHD simulation of cascading reconnection in an extended, global, eruption-generated current layer. We identify the processes that lead to the fragmentation of magnetic and current structures to

smaller elements. Then we analyze the resulting scaling law of the energy cascade. We describe the structure, distribution and dynamics of small dissipation regions embedded in an initially thick current layer. Finally, we discuss the implications that cascading reconnection have for theory of solar flares.

## 2. MODEL

Generally speaking, the solar flare involves three kinds of processes that take place in different scale domains – see Fig 1. At the largest scales magnetic-field energy is accumulated. During this stage flux-rope (filament) is formed and its magnetic energy increases. Eventually it loses its stability and gets ejected. This process already represents (ideal) release of the magnetic-energy at large scales. Subsequently, a current layer is formed and stretched behind ejected flux-rope. Energy transfer from large scales at which the magnetic energy has been accumulated to the small dissipation scale occupies intermediate range of scales. The dissipation itself takes place at smallest, kinetic scales.

In this paper we aim at studying energy transfer from large to small scales by means of numerical simulations. Despite the high spatial resolution our simulation is still within the MHD regime. Also, we do not address the very process of energy accumulation – i.e. the flux-rope formation and energization, nor its instability and subsequent current-layer formation. Instead we assume a relatively thick and extended current layer to be already formed at the initial state of our study. In order to cover a large range of scales we limit ourselves to the 2D geometry allowing for all three components of velocity and magnetic field (commonly referred to as 2.5D models). This is a reasonable assumption since observations show that the typical length of flare arcades along the polarity inversion line (PIL) is much larger than the dimension across the PIL.

In the range of scales that we are interested in the evolution of magnetized plasma can be adequately described by a set of compressible resistive one-fluid MHD equations (e.g. Priest 1984):

$$\begin{aligned} \frac{\partial \rho}{\partial t} + \nabla \cdot (\rho \mathbf{u}) &= 0 \\ \rho \frac{\partial \mathbf{u}}{\partial t} + \rho (\mathbf{u} \cdot \nabla) \mathbf{u} &= -\nabla p + \mathbf{j} \times \mathbf{B} + \rho \mathbf{g} \\ \frac{\partial \mathbf{B}}{\partial t} &= \nabla \times (\mathbf{u} \times \mathbf{B}) - \nabla \times (\eta \mathbf{j}) \\ \frac{\partial U}{\partial t} + \nabla \cdot \mathbf{S} &= \rho \mathbf{u} \cdot \mathbf{g} . \end{aligned} \quad (1)$$

The set of equations (1) is solved by means of Finite Volume Method (FVM). For the numerical solution it is first rewritten in its conservative form. The (local) state of magneto-fluid is then represented by the vector of basic variables  $\Psi \equiv (\rho, \rho \mathbf{u}, \mathbf{B}, U)$ , where  $\rho$ ,  $\mathbf{u}$ ,  $\mathbf{B}$ , and  $U$  are the plasma density, plasma velocity, magnetic field strength and the total energy density, respectively. The energy flux  $\mathbf{S}$  and auxiliary variables – plasma pressure  $p$  and current density  $\mathbf{j}$  – are defined by the formulae:

$$\begin{aligned} \nabla \times \mathbf{B} &= \mu_0 \mathbf{j} \\ U &= \frac{p}{\gamma - 1} + \frac{1}{2} \rho u^2 + \frac{B^2}{2\mu_0} \end{aligned}$$

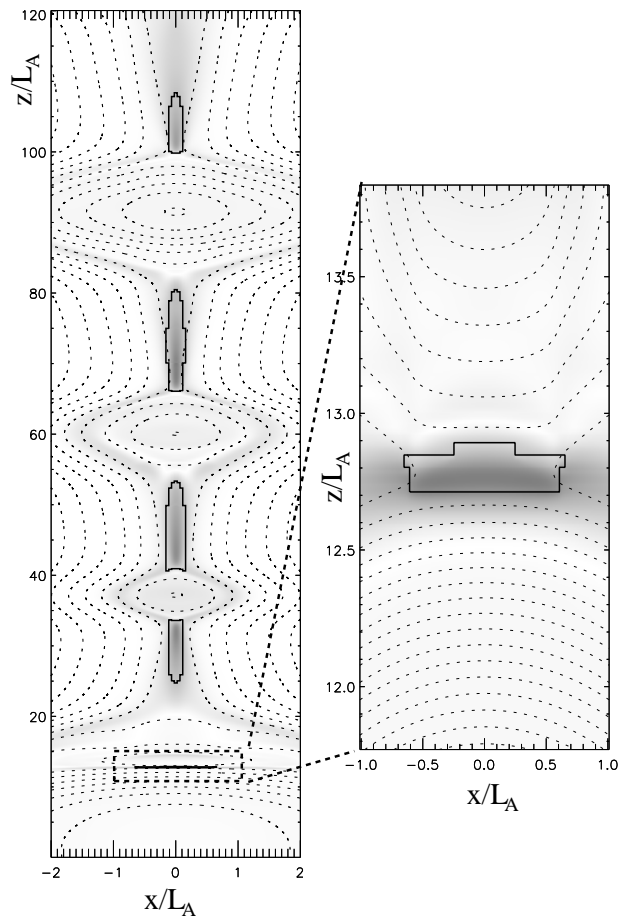


FIG. 2.— Regions of adaptively enhanced resolution (thick-black-line bounded areas) on the background of current density magnitude (gray-scale) and magnetic field lines (dashed). The right panel shows zoomed view of the selected rectangle. Only the relevant sub-set of whole computational domain is shown, note the strongly anisotropic axes-scaling selected in order to show the high-resolution sub-domains better.

$$\mathbf{S} = \left( U + p + \frac{B^2}{2\mu_0} \right) \mathbf{u} - \frac{(\mathbf{u} \cdot \mathbf{B})}{\mu_0} \mathbf{B} + \frac{\eta}{\mu_0} \mathbf{j} \times \mathbf{B} ,$$

and  $\mathbf{g}$  is the gravity acceleration at the photospheric level. Microphysical (kinetic) effects enter into the large-scale dynamics by means of transport coefficients – here via a (generalized) resistivity  $\eta$ . In general, the role of non-ideal terms in the generalized Ohm’s law increases as the current density becomes more concentrated via current sheet filamentation. To quantify this intensification we use the current-carrier drift velocity  $v_D = |\mathbf{j}|/(en_e)$  as the threshold for non-ideal effects to take place. Such behavior is presumed by theoretical considerations and confirmed by kinetic (Vlasov and PIC codes) numerical experiments (Büchner & Elkina 2005, 2006; Karlický & Bárta 2008). In particular, we assume the following law for (generalized) resistivity (see also Kliem et al. 2000):

$$\eta(\mathbf{r}, t) = \begin{cases} 0 & : |v_D| \leq v_{cr} \\ C \frac{(v_D(\mathbf{r}, t) - v_{cr})}{v_0} & : |v_D| > v_{cr} \end{cases} \quad (2)$$

In order to study the energy-transfer cascade it is appropriate to cover a large range of scales. For structured grids it means the utilization of very fine meshes.

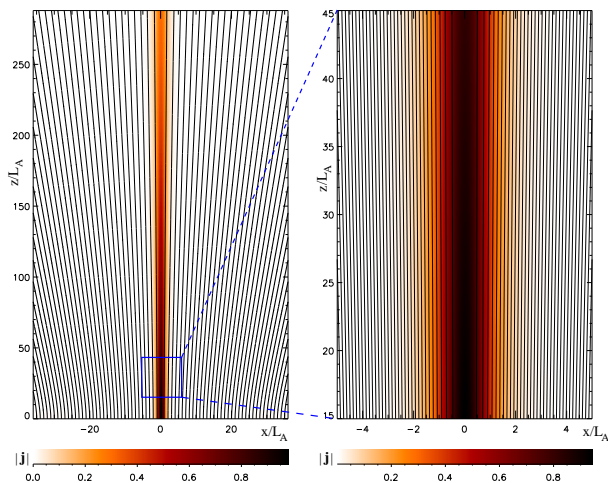


FIG. 3.— Projection of the initial state ( $t = 0$ ) to the  $xz$ -plane. Black lines represent the magnetic field lines, red areas the magnitude of the current density, its scale is given underneath. Enhanced view on selected area (the right panel) can be directly compared with the third panel in Fig. 4.

For a given simulation box size the number of finite grid cells is limited technically by CPU-time and memory demands. Alternatively, one can use a refined mesh only at locations where the small-scale dynamics becomes important – this idea forms the base for the Adaptive Mesh Refinement (AMR) technique (see, e.g., Berger & Oliger 1984; Dreher & Grauer 2005; van der Holst & Keppens 2007). We implemented the numerical solver for the MHD system of equations (1) in the form of block AMR Finite-Volume Method (FVM) code: Whenever the current sheet width drops below a certain threshold, a refined mesh sub-domain is created and initialized with values one step backward in time. Its evolution is then computed using accordingly refined time-step (this procedure is commonly known as sub-cycling). The global dynamics influences the sub-domain evolution by means of time- and spatially varying (interpolated) boundary conditions. For the details of our AMR algorithm see Bárta et al. (2010a). As an illustration, in Fig. 2 the regions of enhanced grid resolution at  $t = 367.0\tau_A$  (for units used see below) are depicted at the background of current density and magnetic field.

The partial differential equations (1) are of a mixed hyperbolic-parabolic type. We utilized the time-splitting approach for their solution: First, hyperbolic (conservative) part is solved using a second-order FVM leap-frog scheme. In a second step the magnetic-diffusivity term is solved by means of a (semi-implicit) Alternating-Direction-Implicit (ADI) scheme (Chung 2002).

We solve the MHD system of Eqs. (1) in a 2D simulation box initially on a global (coarse) Cartesian grid. The horizontal and vertical dimensions of calculated box are 800 and 6400 grid cells, respectively. Using mirroring boundary condition at  $x = 0$  in the symmetric CS (see below) we obtain a doubled box with an effective grid of  $1600 \times 6400$  cells (see also Bárta et al. 2008a, for details). We use the following reference frame: The  $z$ -axis corresponds to the vertical direction, the  $y$ -axis is the invariant (i.e.  $\partial/\partial y = 0$ ) direction along the PIL. The  $x$ -axis is perpendicular to the current layer and cen-

tered at the initial current maximum. The simulation is thus performed in the  $xz$ -plane, while the  $xy$ -plane corresponds to the solar photosphere; the PIL is located at  $x = 0$ ,  $z = 0$  (see Fig. 5 in Bárta et al. 2008a).

The simulation is performed in dimensionless variables. They are obtained by the following normalization: The spatial coordinates  $x$ ,  $y$ , and  $z$  are expressed in units of the current sheet half-width  $L_A$  at the photospheric level ( $z = 0$ ). Time is normalized to the Alfvén-wave transit time  $\tau_A = L_A/V_{A,0}$  through the current sheet, where  $V_{A,0} = B_0/\sqrt{\mu_0\rho_0}$  is the asymptotic value at  $x \rightarrow \infty$  and  $z = 0$  of the Alfvén speed at  $t = 0$ . Eq. (2) for anomalous resistivity in the dimension-less variables then reads  $\eta = C(|\mathbf{j}|/\rho - v_{cr})$  for  $|\mathbf{j}|/\rho > v_{cr}$ .  $C$  and  $v_{cr}$  are now dimension-less parameters. We used  $C = 0.003$  and  $v_{cr} = 15.0$  in our simulation. The choice of the threshold  $v_{cr}$  is not arbitrary as it is closely related to the numeric resolution reached by the code – see the discussion in Section 4. The parameter  $C$  was adjusted to reach peak anomalous resistivities in the order of  $10^6$  times higher than the Spitzer resistivity in the solar corona – similar values for resistivity based on non-linear wave-particle interaction are indicated by Vlasov simulations (Büchner & Elkina 2006).

If not specified otherwise, all quantities in the paper are expressed in this dimension-less system of units. In order to apply our results to actual solar flares appropriate scaling of dimension-less variables, however, has to be performed. The gravity stratification included in our model introduces a natural length scale. Assuming an ambient coronal temperature of  $T = 2$  MK the corresponding scale-height for a fully-ionized hydrogen plasma is  $L_G = 120$  Mm. The value used in our simulation is  $L_G = 200L_A$ , hence  $L_A = 600$  km. For this scaling the flare arcade loop-top is  $\approx 10000$  km high, which corresponds well to observed values. The initial CS width  $2L_A = 1200$  km is roughly in line with the fact that the CS was formed by stretching of the magnetic field in the trail of ejected flux-rope/filament which itself has typical transversal dimensions  $\approx 5000$  km (Vršnak et al. 2009). It also corresponds (by order of magnitude) to estimations made from observations of thin layers trailing behind CMEs that are sometimes interpreted as signatures of current sheets (Ko et al. 2003; Lin et al. 2007). For the ambient magnetic field in the vicinity of the current layer we assume  $B_{z0} = 40$  Gauss (see, e.g., the discussion in Kliem et al. 2000).

The initial state has been chosen in the form of a vertical generalized Harris-type CS with the magnetic field  $\mathbf{B} = \nabla \times \mathbf{A} + \hat{\mathbf{e}}_y B_y$  slightly decreasing with height  $z$  (Bárta et al. 2010a):

$$\begin{aligned} \mathbf{A}(x, y, z; t = 0) &= -B_{z0} \ln \left( e^{\frac{x}{w_{CS}(z)}} + e^{-\frac{x}{w_{CS}(z)}} \right) \hat{\mathbf{e}}_y \\ B_y(x, y, z; t = 0) &= B_{y0}(3) \\ \rho(x, y, z; t = 0) &= \rho_0 \exp\left(-\frac{z}{L_G}\right). \end{aligned}$$

In the following we will refer to  $B_x$  and  $B_z$  as the *principal components* and  $B_y$  as the *guide field*. The characteristic width of the initial current sheet varies with  $z$  as

$$w_{CS}(z) = \frac{d \cdot z^2 + z + z_0}{z + z_0}$$

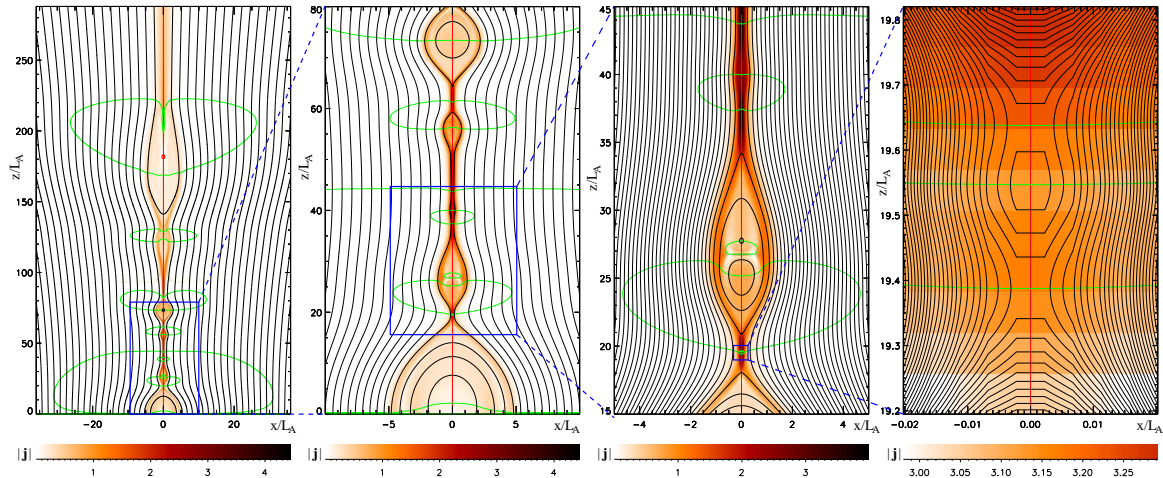


FIG. 4.— Fragmentation of the flare current layer at  $t = 316$ . Increasing zoom reveals further smaller magnetic structures (islands/plasmoids). Red and green lines are positions of  $B_x = 0$ , and  $B_z = 0$ , respectively; their intersections represent the X- and O-type “null” points.

and  $B_{y0}$ ,  $B_{z0}$ ,  $\rho_0$ ,  $d$ , and  $z_0$  are appropriately chosen constants:  $B_{y0} = 0.2$ ,  $\rho_0 = 1.0$ ,  $B_0 = \sqrt{B_{y0}^2 + B_{z0}^2} = 1.0$ ,  $d = 0.003$ , and  $z_0 = 20.0$ . The initial state given by Eq. (3) corresponds to a stratified atmosphere in the presence of gravity (which is consistent with Eqs. (1)). The divergence of the magnetic field-lines towards the upper corona is in agreement with the expansion of the coronal field. It also favors up-ward motion of secondary plasmoids formed in the course of CS tearing (Bárta et al. 2008b). This leads to further filamentation of the current sheets which develop between the plasmoids (Shibata & Tanuma 2001). The current density and magnetic field at the initial state are displayed in Fig. 3. A rather thick current layer is visible. An enhanced view of the selected area is presented in the right panel for the sake of direct comparison with the current-density filamentation developed in later stages of the evolution (see below in Fig. 4).

Free boundary conditions are applied to the upper and right part of the actually calculated right half of the box. It means that von Neumann prescription  $\partial/\partial\mathbf{n} = 0$  has to be fulfilled for all calculated quantities except the normal component of magnetic field  $B_n$  and its contribution to the total energy density  $U$ .  $B_n$  and  $U$  are extended in the second step fulfilling  $\nabla \cdot \mathbf{B} = 0$ . In order to satisfy MHD boundary conditions symmetric ( $q(-z) = q(z)$ ) relations are used for  $\rho$ ,  $B_y$ ,  $B_z$ ,  $U$ , and anti-symmetric ( $q(-z) = -q(z)$ ) for  $B_x$  at the bottom boundary while velocities are set to zero there ( $\mathbf{u} = \mathbf{0}$ ). This ensures that the principal magnetic-field component is vertical at the bottom boundary and that the total magnetic flux passing through that boundary does not change on the rather short time-scales of the eruption, as enforced by the presence of a dense solar photosphere (Bárta et al. 2008a). Mirroring boundary conditions (symmetric in  $\rho$ ,  $u_y$ ,  $B_x$ ,  $B_y$ , and  $U$  and antisymmetric in  $u_x$  and  $B_z$ ) are used for the left part of boundary at  $x = 0$  (=the center of the CS). We use these symmetries to construct (mirror) the left half of the full effective box.

The asymptotic plasma beta parameter at  $x \rightarrow \infty$  and  $z = 0$  is  $\beta = 0.1$  and the ratio of specific heats is  $\gamma = 5/3$

(adiabatic response).

The coarse-mesh sizes are  $\Delta x = \Delta z = 0.045$  in the dimensionless units. Thus, with the reference frame established above the entire box corresponds to  $(-36, 36) \times (0, 288)$  in the  $xz$ -plane. The simulation was performed over 400 normalized Alfvén times. To save disk space only the most interesting interval  $t = 300 - 400$  has been recorded with a step of  $0.5 \tau_A$ .

Note that the initial state described by Eq. (3) is not an exact MHD equilibrium. Nevertheless, the resulting field variations are much weaker than those introduced by reconnection.

At the very beginning, in order to trigger reconnection, the system is perturbed by enhanced resistivity localized in a small region surrounding a line  $x = 0$ ,  $z = 30$  in the invariant direction  $y$  for a short time  $0 \leq t \leq 10$  (see also Magara et al. 1996). This short perturbation sets a localized inflow which somewhat compresses the current layer around the selected point. It should mimic the effect of various irregularities that can be expected during the CS stretching in actual solar eruptions, see also Riley et al. (2007). Later, the resistivity is switched on only if the threshold according to Equation (2) is exceeded. As the threshold for anomalous resistivity cannot be reached for a coarse grid (the threshold for mesh-refinement is reached earlier than the threshold for anomalous resistivity onset), the condition in Eq. (2) is actually checked only at the smallest resolved scale, for the large-scale dynamics we take  $\eta = 0$ .

### 3. ANALYSIS OF MODEL RESULTS

We used the above described numerical code in order to study, which mechanisms are involved in the transfer of free magnetic energy from large to small scales. Thanks to the adaptive mesh we were able to cover scales from  $4.5 \times 10^{-3} L_A$  to  $\approx 300 L_A$  (the larger size of the simulation box), i.e. over almost five orders of magnitude.

The early system evolution can be briefly described as follows: After the localized initial resistivity pulse a flow pattern sets-up that leads to CS stretching (in the  $z$ -) and compression (in the  $x$ -direction). Eventually, the condition in Eq. (2) for anomalous resistivity

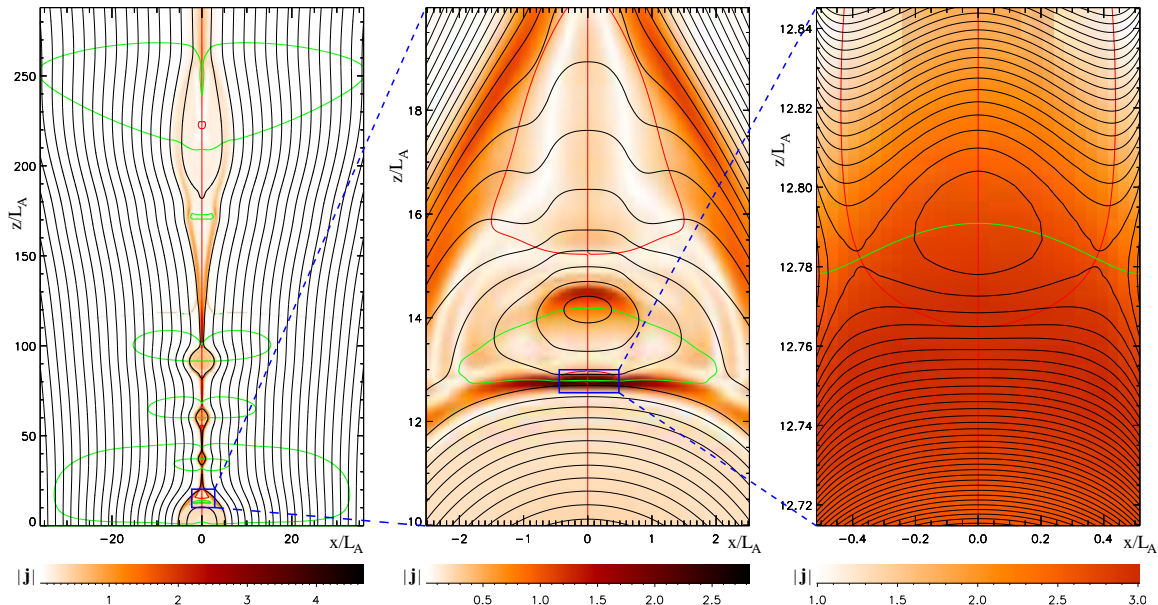


FIG. 5.— Fragmentation of the current layer in the transversal direction at  $t = 367$ . Enhanced zoom reveals further tearing in the transversal (horizontal) current sheet formed due to the mutual interaction (merging/coalescence) between plasmoid and the loop-arcade. Red and green lines are as in Fig. 4.

is reached at the smallest resolved scale and first tearings occur. Dynamics of the plasmoids formed by the tearing process leads to further stretching of CSs interleaving the mutually separating plasmoids. This leads to further generation of tearing. Later, after  $t \approx 300$  the smallest magnetic structures yet consistent with the resolution start appearing. Here we present an analysis of this more developed stage of cascade. Results are shown in Figs. 4 and 5. Fig. 4 shows the state of magnetic field and current density at  $t = 316$ . For better orientation auxiliary lines are added indicating the locations where  $B_x = 0$  and  $B_z = 0$ . Their intersections show the positions of O-type and X-type “nulls” – the points, where only the guide field remains finite. Areas indicated by blue line are consecutively zoomed (from left to right panels). The left-most panel shows the entire simulation box and the right-most corresponds to a zoom at the limit of the AMR-refined resolution. The figure shows, how parts of the current layer are stressed and thinned between separating magnetic islands/plasmoids formed by tearing instabilities. The current-layer filamentation is the most clearly pronounced if one compares the zoomed views of the same selected area at the initial state (Fig. 3, right panel) and the system state at  $t = 316$  (Fig. 4, the third panel). During the dynamic evolution the even thinner, stretched current layers become, after some time, unstable to the next level of tearing and even smaller plasmoids are formed. The zoomed figures show that cascading reconnection has formed plasmoids at the smallest resolved scales: The  $x$ -sizes of the largest and smallest resolved plasmoid in Fig. 4 range from  $\approx 10$  down to  $\approx 0.01$ , the  $z$ -sizes are from  $\approx 0.2$  to  $\approx 70$ .

Plasmoids formed by tearing instability are not only subjected to the separation but they can also approach each other. As a result the magnetic flux piles-up and transversal (i.e. horizontal, perpendicular to the original current layer) current sheets are formed between

pairs of plasmoids approaching each other. Earlier simulations with lower effective resolution treated the plasmoid merging as a coalescence process without any internal structure of the small-scale (sub-grid) current sheet between the magnetic islands since their thickness was not resolved (Tajima et al. 1987; Kliem et al. 2000; Bárta et al. 2008b). If resolved, however, the transversal current sheet does not just dissipate. Instead it is subjected to the tearing instability in the direction perpendicular to the primary current layer. This is shown in Fig. 5. The most detailed resolution (right-most panel) clearly reveals the formation of the O-point at  $x = 0L_A$ ,  $z = 12.79L_A$  and two adjacent X-points at  $x = 0.37L_A$ ,  $z = 12.78L_A$  and  $x = -0.37L_A$ ,  $z = 12.78L_A$ . We call this process “fragmenting coalescence” in order to emphasize that even smaller structures are formed during the merging of two plasmoids. Thus both the tearing and (fragmenting) coalescence processes contribute to the fragmentation of the original thick and smooth current layer.

### 3.1. Fragmentation of CS: Scaling

In order to study scaling properties of the continued fragmentation of the magnetic structures associated with the current layer we performed both a 1D Fourier and a wavelet analysis of the magnetic field along the vertical axis  $\{[x = 0, y = 0, z \in \langle 0, 288 \rangle]\}$ . We use for this study the  $B_x$  component since  $B_z = 0$  there due to the boundary condition. The results are shown in Fig. 6. The upper panel shows the magnetic field and current density in the sub-set of the entire computation domain ( $z \in \langle 0, 200 \rangle$ , note the rotated view), where the current layer is fragmented. Panel (b) shows the profile of  $B_x$  along the current-layer axis, and panels (c) and (d) the Fourier and wavelet analyses of this profile. The Fourier power spectrum exhibits a power-law scaling with the spectral index  $s = -2.14$  in rather wide range of scales

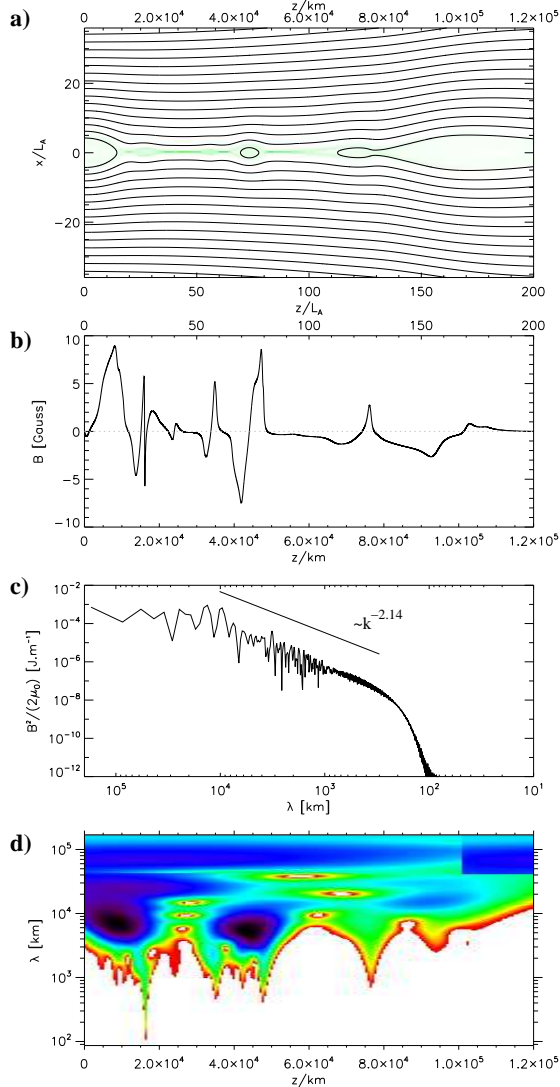


FIG. 6.— The 1D scale analysis of the magnetic field structure along the line  $x = 0$ . (a) Magnetic field lines and the current density structure (green) in the computational domain at  $t = 316$ . The  $z$ -axis shows positions both in the units of  $L_A$  (top) and in kilometers according to scaling adopted in Section 2. (b) Profile of the  $B_x$  component of magnetic field along the line  $x = 0$ . (c) Fourier power spectrum of the  $B_x$  profile. (d) Wavelet power spectrum of the  $B_x$  profile.

300 km – 10000 km. This clearly indicates cascading nature of the continued fragmentation.

The energy-transfer cascade ends at  $\approx 300$  km in Fig. 6. This is closely related to the dissipation threshold  $v_{cr}$  that has been chosen as  $v_{cr} = 15.0$  in our simulation. By selecting this value we shifted dissipation-scale domain into the window of resolved scales – see the discussion in Section 4. Typical width of dissipative current sheets in our model is thus  $L_d \approx L_A/15.0 = 40$  km. Since the plasmoid dimensions along the CS are about one order of magnitude (typically  $6\times$ ) larger than across CS, distribution of magnetic energy in structures along CS, which is depicted in Fig. 6, reaches its dissipation scale at  $\approx 6 \times 40$  km = 240 km. In reality, the ion inertial length  $d_i = c/\omega_{pi}$  is considered as a typical width of dissipative current sheets (Büchner 2007). Its value for

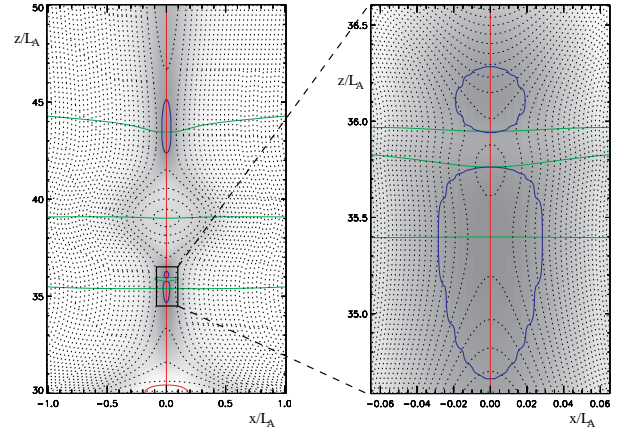


FIG. 7.— Filamentation and splitting of diffusive regions at  $t = 328$ . Detailed treatment shows how the magnetic diffusivity is concentrated into multiple thin channels. The blue-line bounded areas indicate the diffusion regions where the generalized anomalous resistivity (Eq. 2) is finite. Field lines are dashed to be better distinguished from the resistive region boundaries. Current density is represented by gray levels. The right panel displays detailed view of the rectangular box in left. Red and green lines are as in Fig. 4.

parameters  $B_0$  and  $V_A$  used in this paper is  $d_i \approx 4$  m in the simulation-box center, i.e. at  $z \approx 140$  (see Fig. 1).

The most pronounced features in the wavelet spectrum are the locations of low signal (the white islands). They correspond to the filamented parts of the current layer between plasmoids. Their distribution indicates, that the filamented current sheets are embedded within the global current layer in a hierarchical (qualitatively self-similar) manner.

### 3.2. Fragmentation of CS: Diffusion regions

The current sheets are filamented down to the resolution limit of our simulations (in reality to the kinetic scales). The smallest current-density structures contain dissipative/acceleration regions. In the following we will study the structure, distribution and dynamics of these non-ideal regions embedded in the global current layer.

Cascading reconnection and consequent fragmentation of the current layer may have significant impact also for particle acceleration in solar flares. Instead of a single diffusion region assumed in the 'classical' picture of the solar reconnection, cascading fragmentation causes the formation of large amount of thin non-ideal channels. The structuring of non-ideal regions in our simulation is depicted in Fig. 7. The left panel shows two areas of dissipation around  $x = 0$ ,  $z = 36$  and  $x = 0$ ,  $z = 44$ . A closer look (right panel, note the large zoom), however, reveals that the bottom dissipation region is structured and it is in fact formed by two regions of finite magnetic diffusivity that are associated with two X-points at  $x = 0$ ,  $z = 35.40$  and  $x = 0$ ,  $z = 35.97$  interleaved with a (micro) plasmoid. The multiple dissipative regions embedded in the global current layer are favorable for efficient (and possibly multi-step) particle acceleration. At the same time they provide a natural explanation of *fragmented energy release* as it has been inferred from HXR and radio observations (Aschwanden 2002; Karlický et al. 2000). Since they are embedded in the large-scale current layer the 'classical' well-organized

global picture of eruptions is kept simultaneously.

Fig. 7 shows that the X-points formed in the thinned current sheets between magnetic islands are connected with the thin channels of magnetic diffusivity. Hence it is appropriate to study the distribution and dynamics of these non-ideal regions by means of tracking the X-points associated with them. We present such analysis in Fig. 8. In order to see the “skeleton” of the reconnection dynamics we followed the positions of all magnetic “null” points during the entire recorded interval  $t = 300 - 400$ . The results show the kinematics of the O-type (red circles) and X-type points. Motivated by our endeavour to establish a closer relation of the model to observable quantities in our consecutive study (Bárta et al. 2010b) we also paid special attention to the magnetic connectivity of the X-points to the bottom boundary. For this sake, the X-points connected to the model base (= the photosphere) are painted as green asterisks while the unconnected X-points are displayed as black crosses.

Since we are interested in the cascade that already developed into the stage reaching the smallest resolved structures ( $t \geq 300$ ), many X- and O- points connected with the larger-scale (and therefore longer-living) structures (plasmoids) are already formed and their space-time trajectories enter Fig. 8(a) from the bottom. Fig. 8 thus shows mainly full life-cycles of the X- and O- points related to the smallest resolved plasmoids. It is best visible in the three bottom panels (b) – (d) that show zoomed views (projected to the  $zt$ -plane) of typical examples of null-point dynamics – the creation of temporary X–O pairs (panels (b) and (d)) and plasmoid merging (c). As it can be seen from panels (b) and (d) the X-points can become magnetically connected (the right X-point in panel (d)) or disconnected (panel (b)) to/from the bottom boundary during their lifetime. Note also the splitting (and subsequent merging) of the X-point at  $x = 0$ ,  $z = 12.8$  into an X-O-X configuration between  $t \approx 360$  and  $t \approx 380$  in panel (a). This process maps the tearing in the transversal (horizontal) current sheet formed between interacting plasmoid and the loop-arcade (see also Fig. 5). Note that Fig. 8 can be compared with Fig. 5 in Samtaney et al. (2009). The main difference is just in the presence of the off-plane X-points formed by the fragmentation of the CS between coalescing plasmoids in our simulation.

#### 4. DISCUSSION

Reconnection in the trailing current layer behind an ejected flux-rope (filament) is a key feature of the ‘standard’ CSHKP scenario of solar flares. A large amount of free magnetic energy is accumulated around this rather thick (relative to plasma kinetic scales) and very long layer. The thickness of this layer was estimated both from the observed brightening (Ko et al. 2003; Lin et al. 2007) and based on a typical transversal dimensions of a filament (Vršnak et al. 2009). Both ways one obtains the order of magnitude of  $\approx 1000$  km. On the other hand collisionless reconnection requires dissipation at very small scale, thin current sheets with typical width of the order of  $\approx 10$  m in the solar corona (Büchner 2007). The fundamental question arises how the accumulated energy is transferred from large to small scales. Or, in other words, what are the mechanisms of direct energy cascade in magnetic reconnection. We addressed this question using

high-resolution AMR simulation covering broad range of scales to investigate the MHD dynamics of an expanding current layer in the solar corona.

##### 4.1. Mechanisms of direct energy cascade

Our simulations reveal the importance of a continued fragmentation of the current layer due to the interaction of two basic processes: The tearing instability of stretched current sheets and the fragmenting coalescence of flux-ropes/plasmoids formed by the tearing and subsequently forced to merge by the tension of ambient magnetic field. After ejection of the primary flux-rope (i.e. the filament/CME), a trailing current layer is formed behind it which becomes long and thins down. As it has been pointed out by theoretical analysis by Loureiro et al. (2007), current layers with high enough length-to-width ratio become unstable for fast plasmoid instability. Moreover, any irregularity in the plasma inflow that stretches the sheet facilitates the tearing (Lazarian & Vishniac 1999).

Plasmoids that are formed are subjected to the tension of ambient magnetic field, which causes them to move (Bárta et al. 2008b). The motion can lead to their increasing separation. A secondary current layer then formed between them becomes, again, stretched and a secondary tearing instability can take place. This simulation result, illustrated by Fig. 4, fully confirms the scenario suggested by Shibata & Tanuma (2001), developed further by Loureiro et al. (2007) and Uzdensky et al. (2010) into the analytical theory of chain plasmoid instability. The results are also in qualitative agreement with the simulations of plasmoid instability by Samtaney et al. (2009) and Bhattacharjee et al. (2009), which has been performed, however, with constant resistivity.

In addition to that, our simulation has shown that the converging motion of plasmoids leads to a magnetic-flux pile-up between mutually approaching plasmoids. Consequently, secondary (oppositely directed) current sheets are formed perpendicular to the original current layer. While previous studies found only unstructured current density pile-ups between merging magnetic islands our enhanced-by-AMR resolution reveals secondary tearing mode instabilities that take place in the transversal to the primary current sheet direction (see Fig. 5). This process represents a new mechanism of fragmentation and changes our view to coalescence instability, which has been hitherto commonly considered as a simple merging process of two plasmoids contributing to the inverse energy cascade only. Note that this behavior is different from that seen for plasmoids at the dissipation scales in PIC simulations (Drake et al. 2005; Karlický & Bárta 2007), where plasmoids merge without subsequent tearing.

One can suppose that with even higher spatial resolution one would see more subsequent tearing mode instabilities altering with the fragmenting coalescence of the resulting magnetic islands/flux-ropes. As a result third- and higher order current sheets could form.

To sum up, the results of our simulation support the idea that both the tearing (Shibata & Tanuma 2001; Loureiro et al. 2007; Uzdensky et al. 2010) and “fragmenting coalescence” processes lead to the formation of consecutively smaller magnetic structures



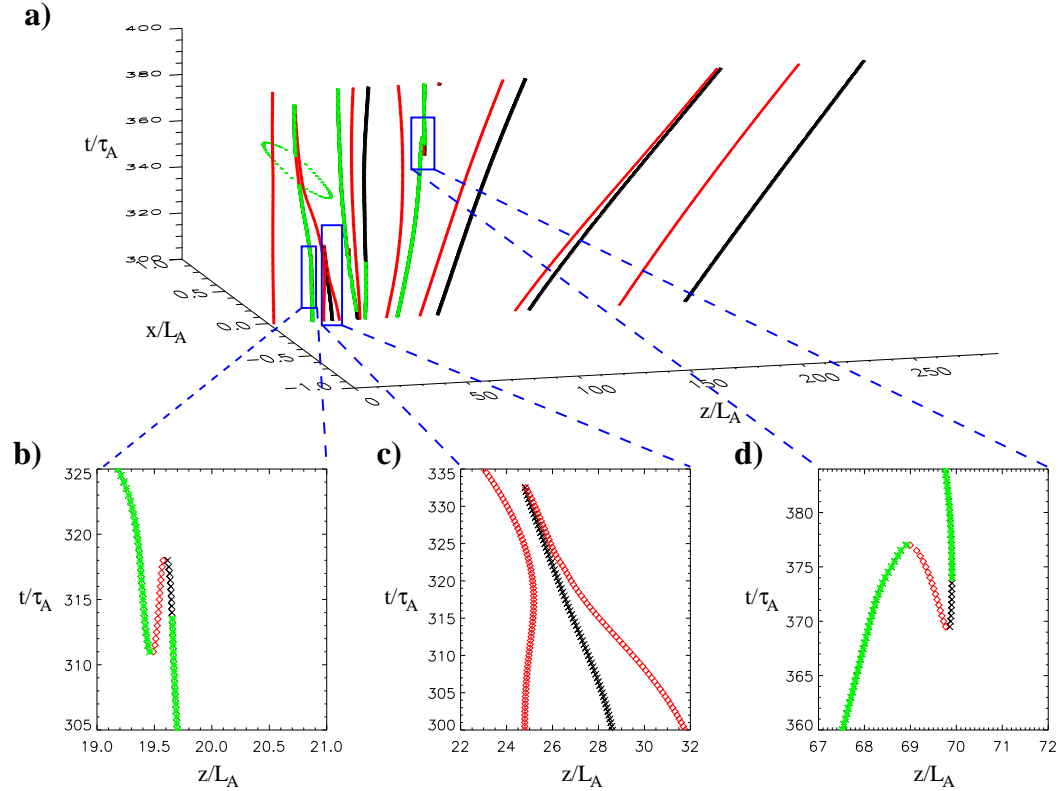


FIG. 8.— Kinematics of the magnetic “null” points (X-points/dissipative regions and O-points/plasmoids). Red circles denote O-point positions, black crosses the X-point positions and green asterisks show the positions of those X-points which are magnetically connected to the photosphere. Three bottom panels show detailed view of selected rectangles and represent typical processes of X- and O-point dynamics: Bifurcation (null-pair creation) and merging (null-pair annihilation).

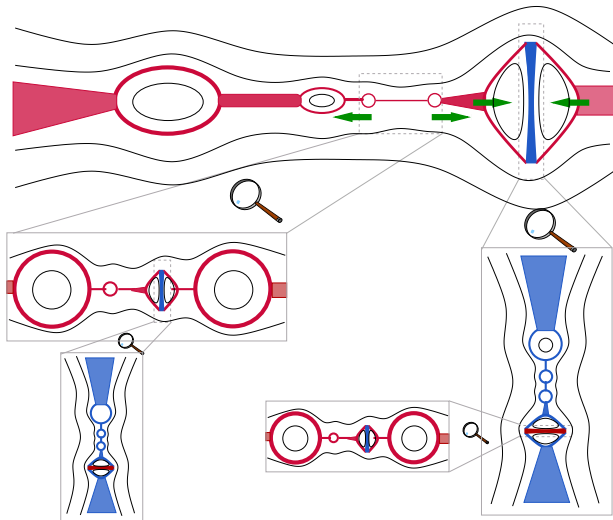


FIG. 9.— Schematic view of cascade of fragmentation of the current layer by tearing and driven coalescence processes. Increasing zoom shows similar kind of processes repeating on smaller scales. Red and blue areas of various hue indicate various intensities of positive and negative out-of-plane ( $j_y$ ) component of current density.

(plasmoids/flux-ropes) and associated current filaments. Subsequent stretching and compression cause a filamentation of the current. This situation is schematically de-

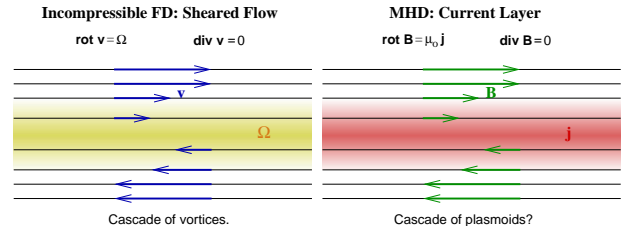


FIG. 10.— Illustration of analogy between sheared-flow in incompressible fluid dynamics (FD) and magnetic reconnection in a large-scale current layers. In the case of FD the mechanism of energy transfer from macroscopic to dissipative (molecular) scale is known – it is the cascade of vortex-tubes. The cascade of magnetic flux-ropes/plasmoids can play this role in the case of magnetic dissipation.

picted in Fig. 9 which can be seen as a generalization of the scheme in Fig. 6. in Shibata & Tanuma (2001). One can expect that this cascade will continue down to the scales where the magnetic energy is, finally, dissipated. Note that the physics and the corresponding scaling laws may change at intermediate (but still relatively small) scales when additional contributions to the generalized Ohm’s law become significant, e.g. a Hall term – see recent simulations by Shepherd & Cassak (2010) and Huang et al. (2010).

#### 4.2. Impact on reconnection efficiency

Reconnection in the current sheet between merging plasmoids is fast since it is driven by ambient-field magnetic tension which naturally pushes the flux-ropes together. Thus even shorter time-scales can be reached by this process than by tearing cascade in the stretched CS (Shibata & Tanuma 2001). And yet another point makes the overall reconnection process more efficient: Many magnetic-flux elements – except those ejected outwards to the escaping CME – reconnect several times. First, during the primary tearing and plasmoid formation and then again during plasmoid coalescence. Since coalescence leads to a follow-up tearing instability (in the transversal direction) the remaining magnetic flux is subjected to another act of magnetic reconnection. This process resembles the *recurrent separator reconnection* simulated by Parnell et al. (2008).

#### 4.3. Relation to turbulence onset

To some extent the initial situation of global, smooth and relatively thick sheets is similar to the turbulence on-set in a sheared flow in (incompressible) fluid dynamics (FD) as schematically shown in Fig. 10. Usually the typical length-scale of shear flows – the counterpart of the width of current layers – is much larger than the dissipative (molecular) scale. The mechanism of energy transfer from large to small scales in classical FD is mediated by a cascade of vortex tubes: Large-scale vortices formed by shear flows can mutually interact giving rise to increased velocity shear at the smaller scales in the space between them. Each small shear flow element formed by this process can be, again, subjected to this fragmentation. Based on our simulation results, we suggest a similar scenario for current-layer fragmentation. The role of the vortex-tubes in FD is in MHD taken over by flux-ropes/plasmoids.

In analogy with the on-set of turbulence in sheared flows, one could expect that a dynamical balance would arise between fragmentation and coalescence processes in later more developed stage. This should be manifested by a power-law scaling rule. Using AMR we reached a rather broad (five orders of magnitude) range of scales. This allowed us to perform a 1D scaling analysis of the magnetic-field structures formed along the current layer for the first time. The scaling rule found exhibits, indeed, a power-law distribution with the index  $s = -2.14$  (Fig. 6). Since our resolution still does not allow to make this scaling analysis only within the small selected sub-domain around the CS center where one could expect isotropic ‘turbulence’ (we would lack sufficient range of scales for that) it is difficult to compare the spectral index found over the whole (clearly anisotropic) simulation domain with the values expected from the theory for fully developed isotropic turbulence.

Obtained power-law distribution is also in qualitative agreement with the concept of fractal reconnection by Shibata & Tanuma (2001) and with hierarchical analytical model of plasmoid instability (Loureiro et al. 2007) as described by Uzdensky et al. (2010). They use distribution functions for plasmoid width and contained flux in order to characterize statistical properties of plasmoid hierarchy rather than power spectrum. We plan to perform similar analysis of our results in the future study in order to compare the results also quantitatively.

In order to obtain as broad as possible scale range

in the plane where reconnection occurs, we performed these simulations using 2.5D approach. The question arises to what extent a full-3D treatment would change the resulting picture. In the FD cascade vortices are deformed, their cross-sections change along their main axis, even in the topological sense. The object defined as a single vortex tube in one place can be split into two in another location. One can expect a similar behavior of plasmoids/flux-tubes in MHD. There they could be subjected to the kink and similar instabilities with  $k_y > 0$ . Such processes would naturally lead to the modulation of reconnection rate along the PIL. Observations indicating such effect have already been presented (McKenzie & Savage 2009). To some extent the expected behavior can also be obtained for kink instabilities of tiny current channels at the dissipative scale studied by 3D PIC simulations (Zhu & Winglee 1996; Karlický & Bárta 2008). Nevertheless, Edmondson et al. (2010) found no such evidence in their 3D AMR MHD simulation, which uses, however, a different set-up. Sizes of the plasmoids formed under 3D perturbation in the direction that corresponds to the invariant  $y$ -axis in our 2.5D case have been found very short preventing a kink-like instabilities to develop. On the other hand, the resulting plasmoid lengths might depend on the initial guide field (Edmondson et al. 2010; Dahlburg et al. 2005).

To sum up, the answer to this question can be found only via full 3D simulations with similar initial set-up as we used here. Therefore we plan to extend our current 2.5D simulations with very high in-plane resolution with moderately resolved structuring in the third dimension.

#### 4.4. Fragmented energy release and particle acceleration

Cascading fragmentation of the current layer is closely related to another puzzling question of current solar flare research – the apparent contradiction between observed regular large-scale dynamics and signatures of fragmented energy release in (eruptive) flares. This duality is reflected by two classes of flare models: The ‘classical’ CSHKP scenario based on magnetic reconnection in a single global flare current sheet and the class of “self-organized criticality” (SOC) models based on the avalanche of small-scale reconnection events in multiple current sheets formed as a consequence of either chaotic (Aschwanden 2002; Vlahos 2007) or regular but still complex boundary motions causing, e.g., magnetic braiding (Wilmot-Smith et al. 2010).

The model of cascading reconnection has the potential to provide a unified view on these seemingly very different (see the discussion in the next paragraph) approaches. From the global point of view, it coincides with the classical CSHKP model keeping the regular picture of the process at large scales. At the same time, due to the *internal* current-layer fragmentation the tearing/coalescence cascade forms multiple small-scale current sheets and potential diffusive regions. As a consequence, fragmented energy release, e.g., by particle acceleration, can take place in these tiny regions. To some extent this finding can be seen as a follow-up of the ‘bursty’ reconnection regime found by Kliem et al. (2000). These authors show that intermittent signal (X-ray, radio) can be related to chaotic pulses of the (resistive) electric field in the dissipation region around X-point. The pulsed

regime is a consequence of non-linear interplay between governing MHD equations and the anomalous resistivity model. In our view, however, these pulses result from the subgrid physics unresolved in earlier simulations. Essentially, what has been seen as a single dissipative region around a single X-point in the coarse-grid models is in fact a (“fractal-like”) set of non-ideal areas around multiple X-points (see Fig. 7) that interleave very small-scale mutually interacting plasmoids. This view based on high-resolved simulation is perhaps closer to the term of “fragmented energy release” that assumes the energy dissipation to be performed via many concurrent small-scale events appearing in multiple sites distributed in space. In this context it is interesting to note how surprisingly well the phenomenological resistivity model (Eq. 2) used by Kliem et al. (2000) mimics the sub-grid scale physics as it has been able to reproduce qualitatively temporal behavior of resistive electric field even without resolving actual processes that are responsible for it. Note also that a possible role of tearing and coalescence in fragmentation of the energy release in solar flares has been mentioned already by Kliem (1990).

We would like to emphasize that there is a fundamental difference between the fragmented energy release by cascading reconnection and SOC models. It is rooted in the fact that in cascading reconnection the complexity/chaoticity is due to an intrinsic current-layer dynamics, i.e., due to spontaneous fragmentation, while it is introduced in SOC models through (external) boundary conditions (chaotic boundary motions). In fact, these two concepts are contrary to some extent: While in SOC-based models the global flare picture is built as an avalanche of many small-scale events (bottom→top process in the scale hierarchy) in cascading reconnection small scale structures are formed as a consequence of internal dynamics of large-scale CS (top→bottom process).

Fragmented energy release is closely related to the number problem of particles accelerated in solar flares. A single diffusion region assumed in the CSHKP model provides a far too small volume for accelerating strong fluxes of particles as they are inferred from the HXR observations. This argument has been used in favor of SOC-based models as they provide energetic-particle spectra and time-profile distributions as observed and explain large energetic particle fluxes.

We suggest that, however, the inclusion of cascading reconnection into the CSHKP has even more capabilities than SOC models. It could explain both the distribution and the number of accelerated particles, based on a physical consideration of many small-scale current sheets which can host tiny diffusive channels that all can act as the acceleration regions (see Fig. 7).

Here it is appropriate to make one technical comment: In an MHD simulation with resistivity model described by Eq. (2), respectively its dimension-less version, the size and the number of diffusive regions are controlled mostly by the threshold  $v_{cr}$  for the onset of (anomalous) diffusivity. The higher  $v_{cr}$  is chosen, the thinner the current sheets can become, the smaller and more numerous are the embedded diffusion regions. Since one has to resolve these diffusive regions in the simulation, one has to

choose the threshold  $v_{cr}$  low enough to be able to resolve the dissipation regions appropriately. In ideally resolved simulations, covering all scales down to the real physical dissipation length, the critical velocity  $v_{cr}$  could be chosen of the order of physically relevant value – the electron thermal speed  $v_{Te}$  (Büchner 2007). In dimensionless units this corresponds to  $v_{cr} = L_A/d_i \sqrt{m_i/m_e} \sqrt{\beta/2}$ , where  $m_i$  and  $m_e$  are the proton and electron masses. For a technically limited spatial resolution, one has to choose a (much) smaller value of  $v_{cr}$  in order to resolve the smallest possible current sheets, before dissipation sets in, by a reasonable number of grid points. Since the resolution in our current AMR simulation is higher than in earlier models, we could choose a more reasonable value of  $v_{cr} = 15.0$  (while older simulations used  $v_{cr} = 3.0$  – see, e.g., Kliem et al. 2000; Bárta et al. 2008a). This allowed us to track down more fragmented, smaller reconnection regions. If we extrapolate this trend, we can expect that with even higher resolution one would find even more and tinier diffusive regions. They would be grouped hierarchically (self-similarly), occupying a sub-space of the global current layer. Such kind of distribution is indicated in the wavelet spectra (white islands in Fig. 6(d)), and also by the positions and motion of the associated X-points in Fig. 8. The latter shows a structured grouping of “null points” and their various life times.

## 5. CONCLUSIONS

Our simulation has shown that cascading reconnection due to the formation and fragmenting coalescence of plasmoids/flux-ropes is a viable physical model of fragmented magnetic energy release in large-scale systems, like solar flares. Cascading reconnection addresses at once three key problems of the current solar-flare research: The scale-gap between energy-accumulation and dissipation scales, the duality between regular global-scale dynamics and fragmented energy-release signatures observed simultaneously in solar flares, and the issue of particle acceleration. All these problems arising from observations appear to be tightly related via cascading reconnection.

In order to evaluate relevance of the cascading reconnection for actual solar flares further it is desirable, however, to identify and predict model-specific observables and to search for them in observed data. We are going to propose possible specific signatures and compare them with observations in a consecutive paper (Bárta et al. 2010b).

This research was performed under the support of the European Commission through the SOLAIRE Network (MTRN-CT-2006-035484) and the grant P209/10/1680 of the Grant Agency of the Czech Republic, by the grant 300030701 of the Grant Agency of the Czech Academy of Science and the research project AV0Z10030501 of Astronomical Institute of the Czech Academy of Science. The authors thank to Dr. Antonius Otto for inspirational discussions and to unknown referee for valuable comments that helped to improve the quality of the paper.

## REFERENCES

- Bárta, M., Büchner, J., Karlický, M., & Kotrč, P. 2010b, *ApJ*, 730, 47, arXiv:1011.6069
- Bárta, M., & Karlický, M. 2001, *A&A*, 379, 1045
- Bárta, M., Karlický, M., & Žemlička, R. 2008a, *Sol. Phys.*, 253, 173
- Bárta, M., Vršnak, B., & Karlický, M. 2008b, *A&A*, 477, 649
- Berger, M. J., & Olinger, J. 1984, *Journal of Computational Physics*, 53, 484
- Bhattacharjee, A., Huang, Y., Yang, H., & Rogers, B. 2009, *Physics of Plasmas*, 16, 112102, arXiv:0906.5599
- Büchner, J. 2006, *Space Science Reviews*, 124, 345
- . 2007, *Plasma Physics and Controlled Fusion*, 49, 325
- Büchner, J., & Elkina, N. 2005, *Space Science Reviews*, 121, 237
- . 2006, *Physics of Plasmas*, 13, 082304.1
- Chung, T. J. 2002, *Computational Fluid Dynamics* (Cambridge University Press, 2002)
- Dahlburg, R. B., Klimchuk, J. A., & Antiochos, S. K. 2005, *ApJ*, 622, 1191
- Drake, J. F., Shay, M. A., Thongthai, W., & Swisdak, M. 2005, *Physical Review Letters*, 94, 095001.1
- Dreher, J., & Grauer, R. 2005, *Parallel Computing*, 31, 913
- Edmondson, J. K., Antiochos, S. K., DeVore, C. R., & Zurbuchen, T. H. 2010, *ApJ*, 718, 72
- Fletcher, L. 2005, *Space Sci. Rev.*, 121, 141
- Huang, Y., & Bhattacharjee, A. 2010, *Physics of Plasmas*, 17, 062104, arXiv:1003.5951
- Huang, Y.-M., Bhattacharjee, A., & Sullivan, B. P. 2010, *ArXiv e-prints*, arXiv:1010.5284
- Karlický, M., & Bárta, M. 2007, *A&A*, 464, 735
- . 2008, *Sol. Phys.*, 247, 335
- Karlický, M., Bárta, M., & Rybák, J. 2010, *A&A*, 514, A28+
- Karlický, M., Jiříčka, K., & Sobotka, M. 2000, *Sol. Phys.*, 195, 165
- Karlický, M., Sobotka, M., & Jiříčka, K. 1996, *Sol. Phys.*, 168, 375
- Kliem, B. 1990, *Astronomische Nachrichten*, 311, 399
- Kliem, B., Karlický, M., & Benz, A. O. 2000, *A&A*, 360, 715, arXiv:astro-ph/0006324
- Kliem, B., Linton, M. G., Török, T., & Karlický, M. 2010, *Sol. Phys.*, 266, 91, arXiv:1007.2147
- Kliem, B., & Török, T. 2006, *Physical Review Letters*, 96, 255002, arXiv:physics/0605217
- Ko, Y., Raymond, J. C., Lin, J., Lawrence, G., Li, J., & Fludra, A. 2003, *ApJ*, 594, 1068
- Krucker, S. et al. 2008, *A&A Rev.*, 16, 155
- Lazarian, A., & Vishniac, E. T. 1999, *ApJ*, 517, 700, arXiv:astro-ph/9811037
- Lin, J., & Forbes, T. G. 2000, *J. Geophys. Res.*, 105, 2375
- Lin, J., Li, J., Forbes, T. G., Ko, Y., Raymond, J. C., & Vourlidas, A. 2007, *ApJ*, 658, L123
- Loureiro, N. F., Schekochihin, A. A., & Cowley, S. C. 2007, *Physics of Plasmas*, 14, 100703, arXiv:astro-ph/0703631
- Magara, T., Mineshige, S., Yokoyama, T., & Shibata, K. 1996, *ApJ*, 466, 1054
- Mandrini, C. H. 2010, in *IAU Symposium 264 "Magnetic energy release: flares and coronal mass ejections"*, eds. A. G. Kosovichev, A. H. Andrei, & J.-P. Roelot, 257–266
- McKenzie, D. E., & Savage, S. L. 2009, *ApJ*, 697, 1569
- Ni, L., Germaschewski, K., Huang, Y., Sullivan, B. P., Yang, H., & Bhattacharjee, A. 2010, *Physics of Plasmas*, 17, 052109
- Parnell, C. E., Haynes, A. L., & Galsgaard, K. 2008, *ApJ*, 675, 1656
- Priest, E. R. 1984, *Solar magneto-hydrodynamics (Geophysics and Astrophysics Monographs, Dordrecht: Reidel, 1984)*
- Riley, P., Lionello, R., Mikić, Z., Linker, J., Clark, E., Lin, J., & Ko, Y. 2007, *ApJ*, 655, 591
- Samtaney, R., Loureiro, N. F., Uzdensky, D. A., Schekochihin, A. A., & Cowley, S. C. 2009, *Physical Review Letters*, 103, 105004, arXiv:0903.0542
- Shepherd, L. S., & Cassak, P. A. 2010, *Physical Review Letters*, 105, 015004, arXiv:1006.1883
- Shibata, K., & Tanuma, S. 2001, *Earth, Planets, and Space*, 53, 473, arXiv:astro-ph/0101008
- Tajima, T., Sakai, J., Nakajima, H., Kosugi, T., Brunel, F., & Kundu, M. R. 1987, *ApJ*, 321, 1031
- Török, T., & Kliem, B. 2005, *ApJ*, 630, L97, arXiv:astro-ph/0507662
- Uzdensky, D. A., Loureiro, N. F., & Schekochihin, A. A. 2010, *Physical Review Letters*, 105, 235002, arXiv:1008.3330
- van der Holst, B., & Keppens, R. 2007, *Journal of Computational Physics*, 226, 925
- Vlahos, L. 2007, in *Lecture Notes in Physics, Berlin Springer Verlag, Vol. 725, "Magnetic Complexity, Fragmentation, Particle Acceleration and Radio Emission from the Sun"*, Berlin Springer Verlag, ed. K.-L. Klein & A. L. MacKinnon, 15–31
- Vršnak, B. et al. 2009, *A&A*, 499, 905, arXiv:0902.3705
- Williams, D. R., Török, T., Démoulin, P., van Driel-Gesztelyi, L., & Kliem, B. 2005, *ApJ*, 628, L163, arXiv:astro-ph/0507661
- Wilmot-Smith, A. L., Pontin, D. I., & Hornig, G. 2010, *A&A*, 516, A5+, arXiv:1001.1717
- Zhu, Z., & Winglee, R. M. 1996, *J. Geophys. Res.*, 101, 4885